Observation of $\chi^{(3)}$-nonlinear optical effects in stimulated Raman scattering (SRS)-active CsLa(WO$_4$)$_2$ crystals: high-order Stokes and anti-Stokes generation and self-Raman CsLa(WO$_4$)$_2$:Nd^{3+} laser converter

A.A. Kaminskii[1,*], O. Lux[2,3,*], H.J. Eichler[2], H. Rhee[2], J. Hanuza[4], M. Ptak[4], J. Dong[5], H. Yoneda[6]

[1] Institute of Crystallography, Center of Crystallography and Photonics, Russian Academy of Sciences, Leninsky prospect 59, 119333 Moscow, Russia
[2] Institute of Optics and Atomic Physics, Technical University of Berlin, 10623 Berlin, Germany
[3] Institute for Atmospheric Physics, German Aerospace Center (DLR), Münchner Str. 20, 82234 Oberpfaffenhofen-Wessling, Germany
[4] Institute of Low Temperature and Structure Research, Polish Academy of Sciences, 50-950 Wroclaw, Poland
[5] School of Information Science and Technology, Xiamen University, Xiamen 361005, P.R. China
[6] Institute for Laser Science, University of Electro-Communications, 182-8585 Tokyo, Japan

E-mail: kaminalex@mail.ru and oliver.lux@dlr.de

Abstract Tetragonal tungstate CsLa(WO$_4$)$_2$:Nd^{3+} was found to be an attractive multifunctional simultaneously Nd^{3+}-laser and SRS-active crystal. A multitude of Stokes and anti-Stokes components is generated in the visible and near-infrared spectral region producing frequency combs with widths of ~8600 cm^{-1} and ~9560 cm^{-1} under pumping at 0.53207 µm and 1.06415 µm wavelength, respectively. All registered nonlinear emission lines are identified and attributed to a single SRS-promoting vibration ν_s(WO$_4$) mode with energy of ω_{SRS} ~ 956 cm^{-1}. Moreover, a passively Q-switched LD-pumped nanosecond self-Raman CsLa(WO$_4$)$_2$:Nd^{3+} laser is reported. An overview of Ln^{3+}-doped tungstate self-Raman lasers is given as well.

Keywords: stimulated Raman scattering (SRS), tungstate crystals, Stokes and anti-Stokes frequency comb, Raman frequency converter, self-Raman laser

1. Introduction

Tungstate crystals play an important role in laser physics and have a long history in nonlinear optics. In particular, one of them, CaWO$_4$:Nd^{3+} became the first laser crystal with trivalent lanthanide (Ln^{3+}) [1]. Currently, there are about 25 tungstate host-crystals with ordered and disordered structure on the basis of which already more than 50 laser crystals doped with Ln^{3+}-ions have been created [2,3], thus enabling the generation of stimulated emission (SE) in the visible and near-IR spectral regions [4]. Many of them are widely used in modern physical experiments, among which the most applicable are monoclinic α-KRE(WO$_4$)$_2$ tungstates (where RE = Y and Ln) whose laser properties were discovered more than 45 years ago by one of us (A.A.K.) [5,6] (see also references for Table 1 in [7]). In addition to their laser potential these monoclinic crystals also have extremely high $\chi^{(3)}$-nonlinearity (thanks to strong symmetric W-O vibration of their [WO$_4$]$^{2-}$ anion groups) which is attractive for exciting high-order stimulated Raman scattering (SRS) as well as for self-SRS lasers as evidenced by Table 1.

1

Table 1. Known multifunctional simultaneously Ln^{3+}-doped laser and SRS-active tungstates[a]

Tungstate[b]	Year of discovery[c]	Space group	Ln^{3+}-lasants[d]	SRS-promoting modes, cm^{-1}	Observed manifestations of $\chi^{(3)}$-nonlinear optical processes
$CaWO_4$	*1961 [1]	$C_{4h}^6 - I4_1/a$	Pr^{3+}, Nd^{3+} [1], Ho^{3+}, Er^{3+}, Tu^{3+}	~908, ~329	SRS [8]
$SrWO_4$	*1963 [9]	$C_{4h}^6 - I4_1/a$	Nd^{3+} [9]	~922	SRS, self-SRS (Nd^{3+})[e], $\chi^{(3)}$-comb[f] [10-12]
$NaLa(WO_4)_2$	*1969 [13]	$C_{4h}^6 - I4_1/a$	Nd^{3+} [13], Tm^{3+}, Yb^{3+}	(923/912)[g], 326.5	SRS [14,27]
$\alpha-KY(WO_4)_2$	*1971 [5,6]	$C_{2h}^6 - C2/c$	Pr^{3+}, Nd^{3+} [5,6], Dy^{3+}, Ho^{3+}, Er^{3+}, Tu^{3+}, Yb^{3+}	~905, ~765, ~87	SRS, self-SRS $(Nd^{3+},Tm^{3+},Yb^{3+})$, $\chi^{(3)}$-comb [15-19]
$\alpha-KGd(WO_4)_2$	*1977 [20]	$C_{2h}^6 - C2/c$	Pr^{3+}, Nd^{3+} [20], Dy^{3+}, Ho^{3+}, Er^{3+}, Tu^{3+}, Yb^{3+}	~901, ~768, ~84	SRS, self-SRS $(Pr^{3+},Nd^{3+},Yb^{3+})$, $\chi^{(3)}$-comb [15,16,21-25]
$\alpha-KEr(WO_4)_2$	*1979 [26]	$C_{2h}^6 - C2/c$	Er^{3+} [26]	~905, ~760	SRS, $\chi^{(3)}$-comb [27]
$\alpha-KLu(WO_4)_2$	*1979 [28]	$C_{2h}^6 - C2/c$	Pr^{3+}, Nd^{3+} [28], Ho^{3+}, Er^{3+}, Tu^{3+}, Yb^{3+}	~907, ~757	SRS, self-SRS (Nd^{3+},Yb^{3+}), $\chi^{(3)}$-comb [3,29-31]
$CsLa(WO_4)_2$	*1988 [32]	$D_{2d}^4 - P\bar{3}2_1c$	Nd^{3+} [32]	~956	SRS[h], self-SRS (Nd^{3+}), $\chi^{(3)}$-comb
$NaBi(WO_4)_2$	*1989 [34]	$C_{4h}^6 - I4_1/a$	Nd^{3+} [33]	~910	SRS, $\chi^{(3)}$-comb [34]
$La_2(WO_4)_3$	*1989 [35]	$C_{2h}^6 - C2/c$	Nd^{3+} [35]	~940	SRS [36]
$NaY(WO_4)_2$	*1998 [37]	$C_{4h}^6 - I4_1/a$	Nd^{3+} [37], Yb^{3+}	~914, ~328	SRS, $\chi^{(3)}$-comb [8,37]
$PbWO_4$	1999 [8]	$C_{4h}^6 - I4_1/a$	Nd^{3+} [8,40]	~901, ~328	SRS, self-SRS (Nd^{3+}), $\chi^{(3)}$-comb [8,38,39]
$ZnWO_4$	1999 [8]	$C_{2h}^4 - P2/c$	Dy^{3+}, Tm^{3+}, Yb^{3+} [41]	~907[i]	SRS [8,40-42]
$BaWO_4$	2000 [43]	$C_{4h}^6 - I4_1/a$	Nd^{3+} [44]	~925, ~332	SRS, self-SRS (Nd^{3+}), $\chi^{(3)}$-comb [43,44]
$\alpha-KYb(WO_4)_2$	*2002 [45]	$C_{2h}^6 - C2/c$	Tm^{3+}, Yb^{3+} [3,45,46]	~907, ~757, ~87	SRS, $\chi^{(3)}$-comb [3]

[a] Here and in the text only articles published in refereed scientific journals are cited.

[b] At room temperature all listed SRS-active tungstates are centrosymmetric crystals and characterized by $\chi^{(3)}$-nonlinearity.

[c] The year of the discovery of Ln^{3+}-laser (indicated by an asterisk) or SRS-effect. To realize the historical stages of these discoveries they are given there in chronological order.

[d] The first Ln^{3+}-lasing ion in this crystal is marked by the corresponding citation.

[e] Self-SRS(Nd^{3+},Yb^{3+}): self-stimulated Raman scattering, i.e., cascaded laser Raman Stokes or(and) anti-Stokes $\chi^{(3)}$-nonlinear generation initiated by SE in Ln^{3+}-doped crystals under external laser pump radiation.

[f] $\chi^{(3)}$-comb: the representation of the spectrum of Stokes and anti-Stokes laser frequency components with a width of at least one octave (i.e., the highest frequency (energy) component must be at least twice of the lowest frequency component).

[g] The energy of SRS-phonons given in [14] requires clarification.

[h] Preliminary information on $\chi^{(3)}$-nonlinear laser activity in a title crystal is reported in [62].

[i] According to [31,40,42] the energy of SRS-phonon was measured as ~906 cm^{-1}.

It presents the known laser multifunctional tungstates and accumulates all observed manifestations of $\chi^{(3)}$-nonlinear processes. This overview table also convincingly reflects the continued interest of researchers in this class of laser crystals crystal throughout the history which is characterized by a remarkably successful advance in physics and nonlinear optics. In this paper, we report the discovery and study of the SRS-effect in tetragonal tungstate $CsLa(WO_4)_2$ single crystals and the first demonstration of a self-SRS laser based on doping this crystal with Nd^{3+}-ions.

2. Crystals for investigations

In our studies, we used crystals of $CsLa(WO_4)_2$ doped with Nd^{3+}-ions ($C_{Nd} \sim 0.5$ and ~2 at. %) for the SRS-experiments, as well as undoped polycrystalline samples of this tungstate for spontaneous Raman scattering spectroscopy. Single crystals were grown by a modified Czochralski method from solution in melts of the polytungstates [32].

Polycrystalline $CsLa(WO_4)_2$ was synthesized from Cs_2CO_3, La_2O_3 and WO_3 of 99.99 % grade. Their mixture with stoichiometric amount was grinded, placed in a crucible and held at ~800°C for 24 h. This process was repeated one again for 24 h at ~850°C. The polycrystalline sample was checked by powder diffraction. Its XRD pattern was the same as presented before [32]. Studies have shown that the $CsLa(WO_4)_2$ crystal belongs to the D_{2d}^4-tetragonal system with unit cell parameters given in Table 2. Its structure contains $[CsO_8]$ and $[LaO_8]$ polyhedra joining each other and forming layers in the *ab*-plane. These layers are bonded through the $[WO_4]$ tetrahedra (see Fig. 1).

Table 2. Some crystallographic and physical properties of tetragonal $CsLa(WO_4)_2$ and $CsLa(WO_4)_2:Nd^{3+}$ single crystals [a]

Characteristics	
Space group (see, e.g. [47])	$D_{2d}^4 - P\bar{3}2_1c$ (No. 114)
Unit-cell parameters, Å [47]	$a = b = 6.552$; $c = 9.640$
Site symmetry (SS) and coordination number (CN) of cations	(Cs^+/La^{3+}): SS – 4e, CN = 8; W^{6+}: SS –8f, CN = 4
Formula units per primitive cell	$Z_{pr} = 2$
Density, g cm^{-3}	~6.16
Melting temperature, °C	~1040
Thermal expansion coefficient, 10^{-6} K^{-1} [48]	$\alpha_{\|a,b} = 26.3$; $\alpha_{\|c} = 8.4$
Nonlinearity	$\chi^{(3)}$
Transmission region [b], μm	~0.35-~5.5
Energy of SRS promoting vibration mode, cm^{-1}	$\omega_{SRS} \sim 956$ [c]
Phonon spectrum extension, cm^{-1}	~ 970 [d]
Spectroscopic-quality parameter, $X = \Omega_4/\Omega_6$ [e]	~ 0.48 [32]
Effective peak cross-section of inter-Stark luminescence transition of Nd^{3+}-laser channel $^4F_{3/2} \rightarrow {}^4I_{11/2}$, 10^{-19} cm^2 [f]	$\sigma_{e,ij}^{eff,p} \sim 1.7$

[a] Most of the data taken from [32].

[b] Averaged statistical data by results of the study double rare-earth multifunctional tungstates (see, e.g. [33,37]).

[c] For $CsLa(WO_4)_2$ crystals doped with Nd^{3+}-ions ($C_{Nd} \sim 2$ at. %).

[d] From spontaneous Raman scattering spectra.

[e] Definition of the spectroscopic-quality parameter is given in [49] (see also Chapter 3 in [2]).

[f] For comparison, the effective pear cross-section for widely used laser crystal $Y_3Al_5O_{12}:Nd^{3+}$ is $\sigma_{e,ij}^{eff,p} \sim 3.3\cdot10^{-19}$ cm^2 (see Table 6.6 in [49]).
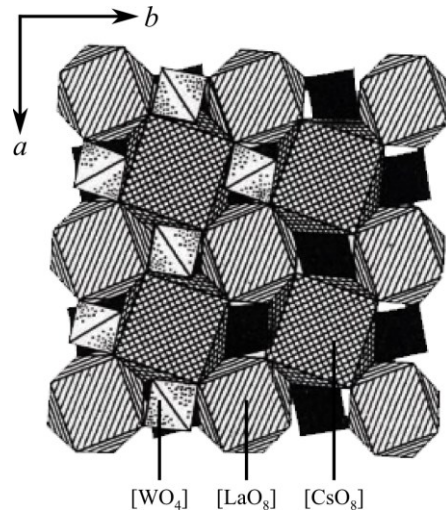

[WO$_4$] [LaO$_8$] [CsO$_8$]

Figure 1. Arrangement of crystal structure of tetragonal $CsLa(WO_4)_2$ [32].

The Nd^{3+} lasant-ions substituting for La^{3+} in the $CsLa(WO_4)_2$ lattice form one kind of activator (lasing) centers. In this case all spectra of Nd^{3+}-ions are characterized by inhomogeneous broadening of the lines due to a partially disordered crystal structure (Cs^+/La^{3+} in 4e crystallographic positions, see Table 2). This explain the luminescence spectra shown in Fig. 2 (left part) and the related Stark-level system Fig. 2 (right part), which determines the lasing properties of its Nd^{3+}-ions.
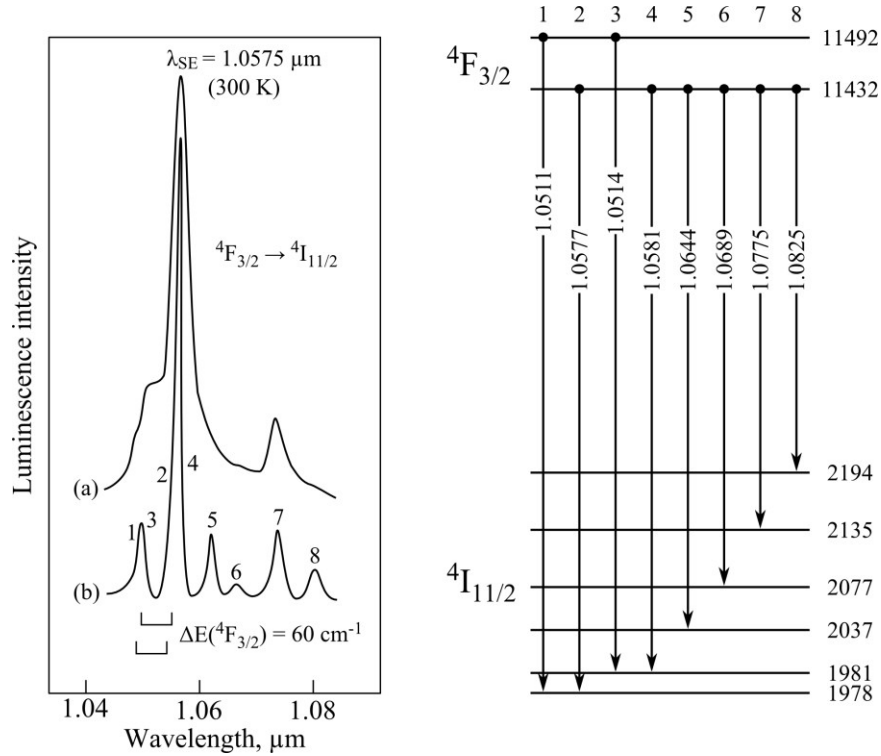

Figure 2. (Left) Luminescence spectra of Nd^{3+}-ions in $CsLa(WO_4)_2$ single crystals at 300 K (a) and 77 K (b). (Right) crystal-field slitting scheme of $^4F_{3/2}$ and $^4I_{11/2}$ manifolds (at 77 K) of Nd^{3+}-ions in $CsLa(WO_4)_2$ single crystal. The Stark level positions are given in cm^{-1}, while the wavelengths of the respective transitions are given in µm [32].
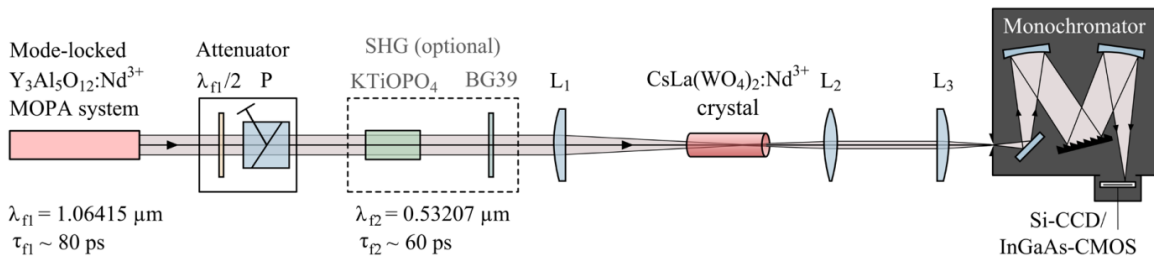

Figure 3. Schematic diagram of the experimental setup used for the spectroscopic analysis of SRS in a $CsLa(WO_4)_2:Nd^{3+}$ single crystal (P: polarizer; L_1-L_3: lenses; see also text).

5

3. $\chi^{(3)}$-nonlinear effects in $CsLa(WO_4)_2$:Nd^{3+} single crystals

The spectroscopic investigation of $\chi^{(3)}$-nonlinear lasing processes in $CsLa(WO_4)_2$:Nd^{3+}($C_{Nd} \sim 0.5$ at.%) was performed using a mode-locked $Y_3Al_5O_{12}$: Nd^{3+} master oscillator power amplifier system in combination with a spectrometric setup as described in previous our publications (see, e.g. [50]). The pump laser system operated at 1 Hz repetition rate, generating single pulses at $\lambda_{f1} = 1.06415$ µm wavelength with pulse energy of up to 40 mJ and pulse duration of about $\tau_{f1} \sim 80$ ps. The pump beam was guided to the registration part of the experimental setup which is shown in Fig. 3.

After propagation through an attenuation stage consisting of a revolving half-wave-plate ($\lambda_{f1}/2$) in combination with a Glan-polarizer (P), the linearly polarized and collimated pump beam could optionally be frequency-doubled using a $KTiOPO_4$ crystal. The second harmonic generation (SHG) process generated $\tau_{f2} \sim 60$ ps pulses at $\lambda_{f2} = 0.53207$ µm wavelength. Suppression of the residual infrared radiation was accomplished by inserting a Schott BG39 filter glass behind the $KTiOPO_4$ doubler which shows a transmission of 0.015% at 1.06415 µm and 96% at 0.53207 µm. The nearly Gaussian beam was then focused into the tungstate crystal by using a plano-convex lens with a focal length of $f_{L1} = 250$ mm. A lens system consisting of a spherical bi-convex lens ($f_{L2} = 100$ mm) and a plano-convex cylindrical lens ($f_{L3} = 100$ mm) collimated the divergent output radiation and imaged it onto the variable entrance slit of a Czerny-Turner monochromator (McPherson Model 270, 6.8 Å/pixel dispersion, 150 lines/mm grating). The spectral composition of the scattered emission was finally recorded by a Si-CCD sensor (Hamamatsu S3924-1024Q with 1024 pixels) for the UV and visible spectral region and an InGaAs sensor (Hamamatsu G9204-512D with 512 pixels) for the range between 0.9 and 1.7 µm, respectively. Two selected recorded $\chi^{(3)}$-lasing spectra are shown in Figs. 4 and 5 and results of an identification of their Stokes and anti-Stokes components are listed in Table 3.
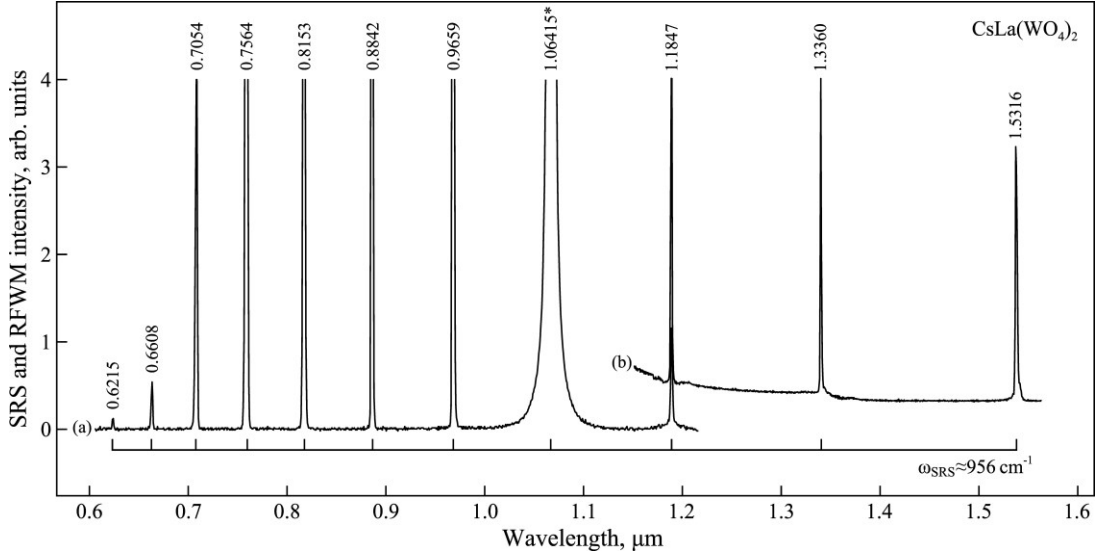
Figure 4. Selected parts of SRS- and RFWM-spectra of a single crystal of $CsLa(WO_4)_2:Nd^{3+}(C_{Nd}$ ~ 0.5 at.%), recorded at room temperature with picosecond pumping at the wavelength λ_{fl} =1.06415 μm in $a(c,c)a$ excitation geometry. The wavelength of all lines (pump line is asterisked) are given in μm, their intensities are shown without correction for the spectral sensitivity of the used multichannel analyzing system. Portion (a) was recorded with a Si-CCD line sensor and portion (b) with an InGaAs-CMOS (their spectral sensitivities are shown in [50]). The energy spacing, related to the SRS-promoting vibration mode ω_{SRS} ~ 956 cm^{-1} of the Stokes and anti-Stokes sidebands spanning a comb of ~1.5 octaves (~9560 cm^{-1}), is indicated by the horizontal scale brackets. The assignment of all recorded nonlinear-lasing lines is given in Table 3.
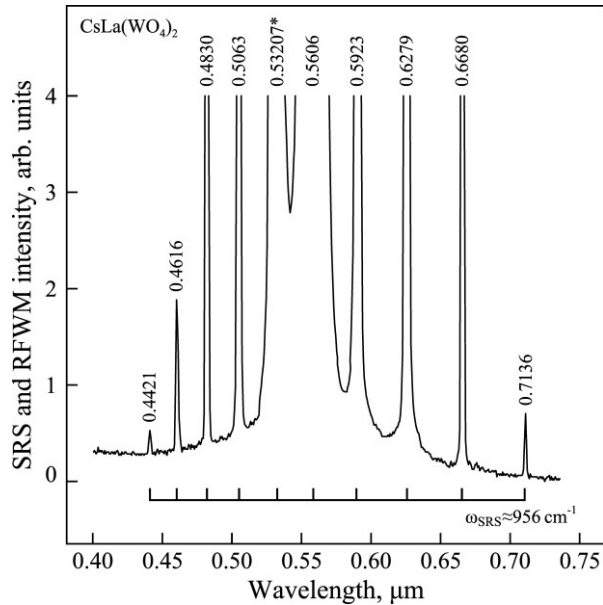

Figure 5. SRS and RFWM spectrum of a single crystal of $CsLa(WO_4)_2:Nd^{3+}(C_{Nd}$ ~ 0.5 at.%), recorded at room temperature with picosecond pumping at the wavelength λ_{f2} = 0.53207 μm in $a(c,c)a$ excitation geometry with a Si-CCD line sensor. The used notations are analogous to that in Fig. 4.

7

Table 3. Spectral composition of the $\chi^{(3)}$-nonlinear lasing in a tetragonal CsLa(WO$_4$)$_2$: Nd^{3+} (C$_{Nd}$ ~ 0.5 at.%), single crystal, related to its single SRS-promoting vibration mode ω_{SRS} ~ 956 cm^{-1}. Data were collected at room temperature under pumping at the fundamental wavelengths λ_{f1} = 1.06415 μm or λ_{f2} = 0.53207 μm (external SHG of λ_{f1}) of a picosecond Y$_3$Al$_5$O$_{12}$:Nd^{3+} pump laser.

Pumping condition		Stokes (St) and anti-Stokes (ASt) lasing		
λ_f, μm	Excitation geometry [a]	Wavelength, μm [b]	Line	$\chi^{(3)}$-nonlinear process [c]
1.06415	$a(c,c)a$ (Fig. 4)	0.6215	ASt$_7\{\lambda_{f1}\}$	$*\omega_{f1}+7\omega_{SRS}=$ $=[\omega_{f1}+(\omega_{f1}+6\omega_{SRS})-(\omega_{f1}-\omega_{SRS})]=$ $=[\omega_{f1}+\omega_{ASt6}-\omega_{St1}]=\omega_{ASt7}$
		0.6608	ASt$_6\{\lambda_{f1}\}$	$*\omega_{f1}+6\omega_{SRS}=$ $=[\omega_{f1}+(\omega_{f1}+5\omega_{SRS})-(\omega_{f1}-\omega_{SRS})]=$ $=[\omega_{f1}+\omega_{ASt5}-\omega_{St1}]=\omega_{ASt6}$
		0.7054	ASt$_5\{\lambda_{f1}\}$	$*\omega_{f1}+5\omega_{SRS}=$ $=[\omega_{f1}+(\omega_{f1}+4\omega_{SRS})-(\omega_{f1}-\omega_{SRS})]=$ $=[\omega_{f1}+\omega_{ASt4}-\omega_{St1}]=\omega_{ASt5}$
		0.7564	ASt$_4\{\lambda_{f1}\}$	$*\omega_{f1}+4\omega_{SRS}=$ $=[\omega_{f1}+(\omega_{f1}+3\omega_{SRS})-(\omega_{f1}-\omega_{SRS})]=$ $=[\omega_{f1}+\omega_{ASt3}-\omega_{St1}]=\omega_{ASt4}$
		0.8153	ASt$_3\{\lambda_{f1}\}$	$*\omega_{f1}+3\omega_{SRS}=$ $=[\omega_{f1}+(\omega_{f1}+2\omega_{SRS})-(\omega_{f1}-\omega_{SRS})]=$ $=[\omega_{f1}+\omega_{ASt2}-\omega_{St1}]=\omega_{ASt3}$
		0.8842	ASt$_2\{\lambda_{f1}\}$	$*\omega_{f1}+2\omega_{SRS}=$ $=[\omega_{f1}+(\omega_{f1}+\omega_{SRS})-(\omega_{f1}-\omega_{SRS})]=$ $=[\omega_{f1}+\omega_{ASt1}-\omega_{St1}]=\omega_{ASt2}$
		0.9659	ASt$_1\{\lambda_{f1}\}$	$*\omega_{f1}+\omega_{SRS}=$ $=[\omega_{f1}+\omega_{f1}-(\omega_{f1}-\omega_{SRS})]=$ $=[\omega_{f1}+\omega_{f1}-\omega_{St1}]=\omega_{ASt1}$
		1.06415	λ_{f1}	ω_{f1}
		1.1847	St$_1\{\lambda_{f1}\}$	$\omega_{f1}-\omega_{SRS}=\omega_{St1}$
		1.3360	St$_2\{\lambda_{f1}\}$	$*\omega_{f1}-2\omega_{SRS}=$ $=(\omega_{f1}-\omega_{SRS})-\omega_{SRS}=\omega_{St2}$
		1.5316	St$_3\{\lambda_{f1}\}$	$*\omega_{f1}-3\omega_{SRS}=$ $=(\omega_{f1}-2\omega_{SRS})-\omega_{SRS}=\omega_{St3}$

0.53207	$a(c,c)a$ (Fig. 5)	0.4421	$ASt_4\{\lambda_{f2}\}$	$*\omega_{f2}+4\omega_{SRS}=$ $=[\omega_{f2}+(\omega_{f2}+3\omega_{SRS})-(\omega_{f2}-\omega_{SRS})]=$ $=[\omega_{f2}+\omega_{ASt3}-\omega_{St1}]=\omega_{ASt4}$
		0.4616	$ASt_3\{\lambda_{f2}\}$	$*\omega_{f2}+3\omega_{SRS}=$ $=[\omega_{f2}+(\omega_{f2}+2\omega_{SRS})-(\omega_{f2}-\omega_{SRS})]=$ $=[\omega_{f2}+\omega_{ASt2}-\omega_{St1}]=\omega_{ASt3}$
		0.4830	$ASt_2\{\lambda_{f2}\}$	$*\omega_{f2}+2\omega_{SRS}=$ $=[\omega_{f2}+(\omega_{f2}+\omega_{SRS})-(\omega_{f2}-\omega_{SRS})]=$ $=[\omega_{f2}+\omega_{ASt1}-\omega_{St1}]=\omega_{ASt2}$
		0.5063	$ASt_1\{\lambda_{f2}\}$	$*\omega_{f2}+\omega_{SRS}=$ $=[\omega_{f2}+\omega_{f2}-(\omega_{f2}-\omega_{SRS})]=$ $=[\omega_{f2}+\omega_{f2}-\omega_{St1}]=\omega_{ASt1}$
		0.53207	λ_{f2}	ω_{f2}
		0.5606	$St_1\{\lambda_{f2}\}$	$\omega_{f2}-\omega_{SRS}=\omega_{St1}$
		0.5923	$St_2\{\lambda_{f2}\}$	$*\omega_{f2}-2\omega_{SRS}=$ $=(\omega_{f2}-\omega_{SRS})-\omega_{SRS}=\omega_{St2}$
		0.6279	$St_3\{\lambda_{f2}\}$	$*\omega_{f2}-3\omega_{SRS}=$ $=(\omega_{f2}-2\omega_{SRS})-\omega_{SRS}=\omega_{St3}$
		0.6680	$St_4\{\lambda_{f2}\}$	$*\omega_{f2}-4\omega_{SRS}=$ $=(\omega_{f2}-3\omega_{SRS})-\omega_{SRS}=\omega_{St4}$
		0.7136	$St_5\{\lambda_{f2}\}$	$*\omega_{f2}-5\omega_{SRS}=$ $=(\omega_{f2}-4\omega_{SRS})-\omega_{SRS}=\omega_{St5}$

[a] Notation is used in analogy to that in [54]. The characters to the left and to the right of the brackets give the direction of the wave normal of the pumping and the nonlinear generation wave, respectively, while the characters between the brackets indicate (from left to right) the polarization direction of the pumping and nonlinear generated wave, respectively.

[b] Measurement accuracy ±0.0003 μm.

[c] Lines related to the cascaded $\chi^{(3)}$-nonlinear processes are asterisked. In square brackets three different possible Raman four-wave mixing (RFWM) processes for the generation of the respective nonlinear component are given.

4. Spontaneous Raman spectra of polycrystalline CsLa(WO$_4$)$_2$

FT Raman spectra of polycrystalline $CsLa(WO_4)_2$ in the 1000-70 cm^{-1} range were measured using a Bruker FT-Raman RFS 100/S spectrometer and under CW excitation emission of $Y_3Al_5O_{12}:Nd^{3+}$ laser at 1.06415 μm wavelength. The measurements were performed in the backscattering configuration. The spectral resolution was ~2 cm^{-1}. These spectra were compared to those recorded on a Renishaw InVia Raman spectrometer equipped with a confocal DM 2500 Leica optical microscope, a

thermoelectrically cooled Ren Cam CCD as a detector and Ar^+-ion laser operating at 0.488 μm wavelength. To our knowledge, Raman spectra of this compound were not measured and analysed in terms of its possible structure. In few papers, it was proposed alternatively as tetragonal $D_{4h}^{15} - P4_2/nmc$ [52-55] or $D_{2d}^4 - \overline{P}42_1c$ [47]. It was also postulated that it is isostructural with α-RbLa$(MoO_4)_2$ described in $D_{4h}^4 - P4/nnc$ space group [56,59]. As noted above, it was postulated that CsLa$(WO_4)_2$ consists of joined [CsO$_8$] and [LaO$_8$] polyhedra forming layers in the *ab*-plane (see Fig. 1). These layers are bonded through the [WO$_4$] tetrahedra. These data could be verified in the present paper when the Raman spectra of this compound became available. The first order spontaneous Raman scattering spectrum of polycrystalline CsLa$(WO_4)_2$ is shown in Fig. 6. The wavenumbers of the observed bands are used in the present work in the analysis of the SRS spectra of this material. CsLa$(WO_4)_2$ crystallizing in the above described structures contains two molecules in the primitive unit cell (Z_{pr} = 2), i.e. two Cs^+, two La^{3+}, four W^{6+} and sixteen O^{2-}-ions. 24 atoms of the primitive cell give rise to $3NZ_{pr}$ = 72 zone-center degrees (at κ = 0) of freedom described by the irreducible representations related to particular ions. They are listed in Table 4.
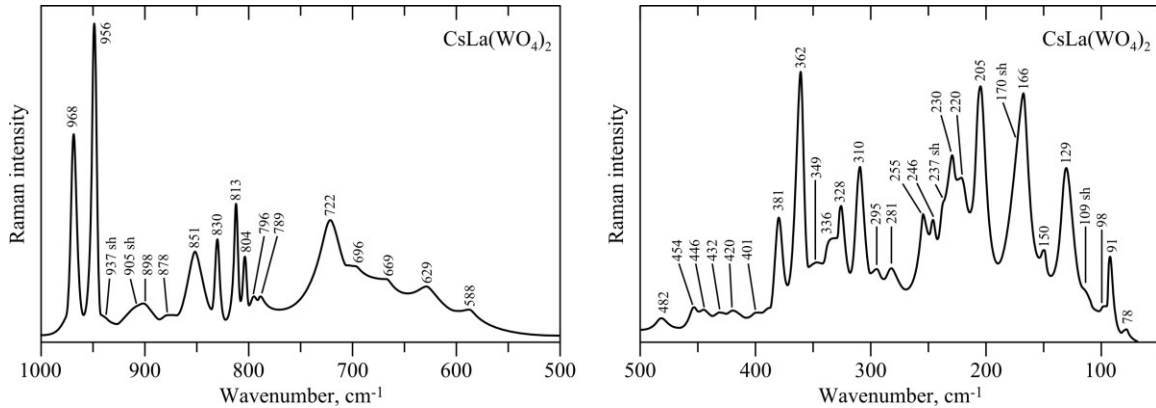

Figure 6. Spontaneous Raman scattering spectra of CsLa$(WO_4)_2$ in polycrystalline state.

Table 4. Contribution of respective ions of particular unit cells to the irreducible representations of the vibrational degrees of freedom.

Ion	P4/nnc	P4$_2$/nmc	$\overline{P}42_1c$
$\Gamma(La^{3+})$	$A_{2g}+A_{2u}+E_u+E_g$	$A_{2u}+B_{1g}+E_u+E_g$	B_1+B_2+2E
$\Gamma(Cs^+)$	$A_{2g}+A_{2u}+E_u+E_g$	$A_{2u}+B_{1g}+E_u+E_g$	B_1+B_2+2E
$\Gamma(W^{6+})$	$A_{1u}+A_{2u}+B_{1g}+B_{2g}+$ $+2E_u+2Eg$	$A_{1g}+A_{2u}+B_{1g}+2E_u+2E_g$	$A_1+A_2+B_1+B_2+4E$
$\Gamma(O^{2-})$	$3A_{1g}+3A_{1u}+3A_{2g}+$ $+3A_{2u}+3B_{1g}+3B_{1u}+$ $+3B_{2g}+3B_{2u}+6E_u+6E_g$	$3A_{1g}+3A_{1u}+3A_{2g}+3A_{2u}+$ $+3B_{1g}+3B_{1u}+3B_{2g}+3B_{2u}+$ $+6E_u+6E_g$	$5A_1+5A_2+5B_1+5B_2+$ $+14E$
Γ_Σ	$3A_{1g}+4A_{1u}+5A_{2g}+$ $+6A_{2u}+4B_{1g}+3B_{1u}+$ $+4B_{2g}+3B_{2u}+10E_u+$ $+10E_g$	$4A_{1g}+3A_{1u}+3A_{2g}+6A_{2u}+$ $+6B_{1g}+3B_{1u}+3B_{2g}+4B_{2u}+$ $+10E_u+10E_g$	$6A_1+6A_2+8B_1+8B_2+$ $+22E$
$\Gamma_{optical}$	$3A_{1g}+4A_{1u}+5A_{2g}+$ $+5A_{2u}+4B_{1g}+3B_{1u}+$ $+4B_{2g}+3B_{2u}+9E_u+$ $+10E_g$	$4A_{1g}+3A_{1u}+3A_{2g}+5A_{2u}+$ $+6B_{1g}+3B_{1u}+3B_{2g}+4B_{2u}+$ $+9E_u+10E_g$	$6A_1+6A_2+8B_1+7B_2+$ $+21E$
$\Gamma_{acoustic}$	$A_{2u}+E_u$	$A_{2u}+E_u$	B_2+E
Raman activity	A_{1g}, B_{1g}, B_{2g}, E_g	A_{1g}, B_{1g}, B_{2g}, E_g	A_1, B_1, B_2, E
Number of Raman bands	21	23	44

Analyzing the results of theoretical calculations performed for three possible unit cells postulated for CsLa(WO$_4$)$_2$, it is seen that the number of Raman bands expected for P4/nnc structure is 21, for P4$_2$/nmc structure it is 23 and for the $\overline{P}42_1c$ structure it is 44. On the other hand, the number of bands observed in the Raman spectrum (Fig. 6) is 45 what means that most the structure of the studied material is most probably described by the $\overline{P}42_1c$ space group. This result should be confirmed by the measurements of the polarized IR and Raman spectra of the single crystal. Analyzing the intensity of the bands

observed in the spontaneous Raman spectrum the strongest lines appear at ~956, ~362, and ~230 cm^{-1}. These bands correspond to the following phonons: symmetric stretching $\nu_s(WO_4)$, symmetric bending $\delta_s(WO_4)$ and translation $T(WO_4)$ of the A_1 symmetry. Other strong bands observed at ~956, ~205, and ~166 cm^{-1} should be assigned to phonons of B_1 symmetry. The latter two correspond to the translations $T(La^{3+})$ and $T(Cs^+)$. The strongest line in the spontaneous Raman spectrum at ~956 cm^{-1} is responsible for observed SRS-effect in studied crystal.

5. Self-SRS lasing in a $CsLa(WO_4)_2:Nd^{3+}$ crystal

The study of $\chi^{(3)}$-nonlinear properties of tetragonal $CsLa(WO_4)_2:Nd^{3+}$ crystal also revealed its ability for self-SRS lasing. The title crystal, as well as other known Ln^{3+}-laser and SRS-active double rare-earth tungstates, is characterized by a relatively high first-Stokes Raman gain coefficient (not less than 2 cm·GW^{-1} at 1.06415 μm, see, e.g. [8,18,43,57]). In addition, the effective peak cross-section of the inter-Stark luminescence transition of Nd^{3+}-laser channel $^4F_{3/2} \rightarrow {}^4I_{11/2}$ also shows a fairly large value $\sigma_{e,ij}^{eff,p}$ ~ 1.7·10^{-19} cm^2 (see, Table 1). These factors have stimulated the investigation of self-SRS generation in $CsLa(WO_4)_2:Nd^{3+}$ (C_{Nd} ~ 2 at.%) in order to demonstrate its laser multifunction capabilities. It was carried out by deploying the Q-switch laser setup shown in Fig. 7. Its scheme is characterized by its operational simplicity and is thus widely used in many research laboratories (see, e.g. [41,58-61]). Here, we only mention the main features of the setup which included a commercial CW fiber-coupled LD (LIMO GmbH) as pump source providing up to 4 W of pump power at $\lambda_p = 0.81$ μm wavelength. A polished ~0.8 mm-thick plate made from a "black garnet" ($Y_3Al_5O_{12}$:Ca,Cr) crystal acted as a saturable absorber (SA) with an initial transmission of 90% at the (fundamental) wavelength $\lambda_{SE} = 1.0575$ μm, generating single pulses with duration of ~2 ns at 16 kHz repetition rate. First-order Stokes lasing at $\lambda_{St1} = 1.1765$ μm wavelength was realized by selective amplification of this Raman component in the 40 mm-long laser resonator while confining the fundamental field in the cavity (see mirror reflectivities in Table 5). Under these experimental conditions the self-SRS lasing spectrum of a $CsLa(WO_4)_2:Nd^{3+}$ crystal was recorded, which is shown in Fig. 8.
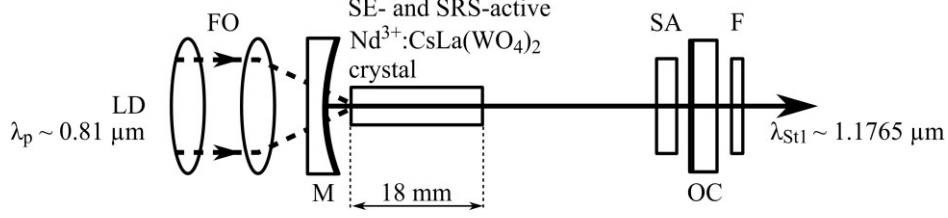
Figure 7. Experimental setup for pumped Q-switched CsLa(WO$_4$)$_2$:Nd^{3+} nanosecond self-SRS laser through the nonlinear cascade steps SE ($\lambda_{SE} \sim 1.0575$ µm, $^4F_{3/2} \to {}^4I_{11/2}$) $\to$ SRS ($\lambda_{St1} \sim 1.1765$ µm, $\omega_{SRS} \sim 956$ cm^{-1}): LD, CW fiber-coupled laser diode; FO, focusing optics; M: concave "pump" mirror; SA, (Y$_3$Al$_5$O$_{12}$:Ca,Cr) saturable absorber; OC, flat output coupler having dichroic multilayer coatings; F, filter.

Table 5. Reflection (R) and transmission (T) of the CsLa(WO$_4$)$_2$ self-Raman laser cavity mirrors at the fundamental wavelength λ_{SE}, the first Stokes wavelength λ_{St1} and the pump wavelength λ_p.

Wavelength, µm	R_M, %	T_M, %	R_{OC}, %	T_{OC}, %
$\lambda_{SE} \sim 1.0575$ µm	~99.2	[a]	~99.5	[a]
$\lambda_{St1} \sim 1.1765$ µm	~99.5	[a]	~58	~40
$\lambda_p \sim 0.81$ µm	~15	~85	~10	[b]

[a] Minor transmission (<1%).
[b] The CsLa(WO$_4$)$_2$ crystal absorbs almost 100% of the pump radiation.

Due to the high intra-cavity losses introduced by the uncoated crystal end-faces, crystal impurities and the saturable absorber, the overall conversion efficiency from the pump at $\lambda_p = 0.81$ µm wavelength to the first Stokes at $\lambda_{St1} = 1.1765$ µm wavelength was only a few percent. We expect that much higher conversion efficiency can be obtained by using anti-reflection-coated commercial crystals with higher optical quality and by optimizing the cavity specifications, i.e. mirror reflectivities and curvatures, of the self-Raman laser. This experiment was the first realization of a self-SRS laser based on a tetragonal CsLa(WO$_4$)$_2$:Nd^{3+} crystal. The laser hence became the seventh representative from the group of tungstate self-Raman lasers (see Table 1). Our further investigation will aim at obtaining cascaded $\chi^{(3)}$-nonlinear generation at ~1.5234 µm wavelength involving the other strong intermanifold $^4F_{3/2} \to {}^4I_{13/2}$ transition of the Nd^{3+}-lasant ion in CsLa(WO$_4$)$_2$:Nd^{3+} at ~ 1.3297 µm. Laser emission in this so-called "eye-safe" spectral region is of particular interest for remote sensing and medical applications. In this context, it is appropriate to note that the crystal has the highest Raman frequency shift (~956 cm^{-1}) of all known SRS-active tungstates (see Table 1), thus facilitating the access to the eye-safe region via a single SRS conversion step.
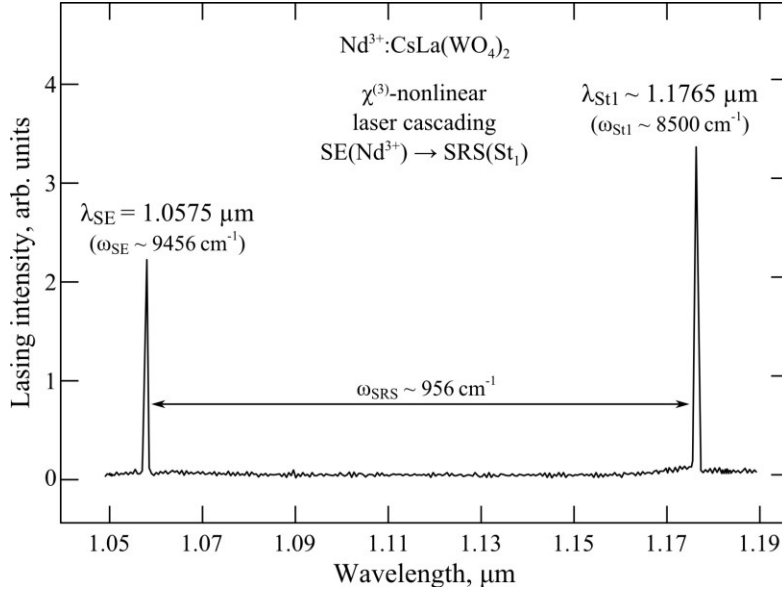
Figure 8. Room-temperature $\chi^{(3)}$-nonlinear Q-switched of nanosecond CsLa(WO$_4$)$_2$:Nd^{3+} self-SRS lasing spectrum recorded with a grating AQ-type spectra analyzer equipped with a fast InGaAs PIN-photodiode and a digital Tektronix oscilloscope.

5. Conclusion

In this study, the $\chi^{(3)}$-nonlinear optical potential of tetragonal CsLa(WO$_4$)$_2$:Nd^{3+} single crystals was revealed by means of steady-state picosecond SRS-spectroscopy. The tungstate was demonstrated to be a promising crystalline material for both broadband Stokes and anti-Stokes generation from the blue to near-IR spectral range and self-Raman lasing at 1.1765 μm wavelength involving a single SRS-active vibration mode with ω_{SRS} ~ 956 cm^{-1}. We hope that the results of this work will help to address some practical tasks of modern laser physics.

References

[1]   Johnson L F and Nassau K 1961 *Proc. IRE* **49** 1704

[2]   Kaminskii A A 1996 *Crystalline Lasers: Physical Processes and Operating Schemes* (Boca Raton, FL: CRC Press)

[3]   Kaminskii A A 2007 *Laser Photonics Rev.* **1** 93

[4]   Weber M J 2000 *Handbook of Laser Wavelengths* (Boca Raton, FL: CRC Press)

[5]   Kaminskii A A, Klevtsov P V and Pavlyuk A A 1971 *Phys. Status Solidi* a **5** K79

[6]   Kaminskii A A, Klevtsov P V, Li L and Pavlyuk A A 1971 *IEEE J. Quantum Electron.* **8** 457

[7]   Kaminskii A A *et al* 2002 *Phys. Rev.* B **65** 125108

[8]   Kaminskii A A *et al* 1999 *Appl. Opt.* **38** 4533

[9]   Johnson L F 1963 *J. Appl. Phys.* **34** 897

[10]   Kaminskii A A, Bagaev S N, Ueda K, Takaichi K and Eichler H J 2002 *Crystallogr. Rep.* **47** 653

[11]   Breneir A, Jia G and Tu C 2004 *J. Phys.: Condens Matter* **16** 9103

[12]   Jelnikova J, Sulc J, Basiev T T, Zverev P G and Kravtsov S V 2005 *Laser Phys. Lett.* **2** 4

[13]   Kaminskii A A, Kolodnyi G Y and Sergeeva N A 1968 *J. Appl. Spectrosc.* **9** 1275

[14]   Garcia-Cortés A, Cascales C, deAndrés A, Zaldo C, Zharikov E V, Subbotin K A, Bjurshagen S, Pasiskevicius V and Rico M 2007 *IEEE J. Quantum Electron.* **43** 157

[15]   Andryunas K, Vishkas Y, Kobelka V, Mochalov I V, Pavlyuk A A, Petrovskii G T and Syrus V 1985 *JETP Lett.* **42** 410

[16] Kaminskii A A, Nishioka H, Kubota K, Ueda K, Takuma H, Bagaev S N and Pavlyuk A A 1995 *Phys. Status Solidi* a **148** 619

[17]   Wu L, Wang A, Wu J, Wei L, Zhu G and Ving S 1995 *Electron. Lett.* **31** 1151

[18]   Kaminskii A A, Konstantinova A F, Orechova V P, Butashin A V, Klevtsova R E and Pavlyuk A A 2001 *Crystallogr. Rep.* **46** 665

[19]   Demidovich A A, Grabtchenko A S, Kuzmin A N, Lisnitskii V A and Orlovich V A 2002 *Eur. Phys. J. Appl. Phys.* **19** 113

[20]   Kaminskii A A, Pavlyuk A A, Klevtsov P V, Balashov I F, Berenberg V A, Sarkisov S E, Fedorov V A, Petrov M V and Lyubchenko V V 1977 *Inorg. Mater.* **13** 482

[21]   Ivanyuk A M, Shakhverdov P A, Belyaev V D, Ter-Pogosyan M A and Ermolaev V L 1985 *Opt. Spectrosc.* **58** 967

[22]   Kaminskii A A, Ustimenko N S, Gulin A V, Bagaev S N and Pavlyuk A A 1998 *Dokl.-Phys.* **43** 2148

[23] Gulin A V, Narchova G I and Ustimenko N S 1998 *Quantum. Electron.* **28** 804

[24] Legatskii A A, Abdolvand A and Kuleshov N V 2000 *Opt. Lett.* **25** 616

[25] Omatsu T, Ojima Y, Pask H M, Piper J A and Dekker P 2004 *Opt. Commun.* **232** 327

[26] Kamnskii A A, Pavlyuk A A, Butaeva T I, Bobovich L I and Lyubchenko V V 1979 *Inorg. Mater.* **15** 424

[27] Becker P, Bohatý L, Eichler H J, Rhee H and Kaminskii A A 2007 *Laser Phys. Lett.* **4** 884

[28] Kamnskii A A, Pavlyuk A A, Agamalyan N P, Sarkisov S E, Bobovich L I, Lukin A V and Lyubchenko V V 1979 *Inorg. Mater.* **15** 16

[29] Kaminskii A A, Ueda K, Eichler H J, Findeisen J, Bagayev S N, Kusnetsov F A, Pavlyuk A A, Boulon G and Bourgeois F 1998 *Japan. J. Appl. Phys.* **37** L923

[30] Liu J, Griebner U, Petrov V, Zhang H, Zhang J and Wang J 2005 *Opt. Lett.* **30** 2427

[31] Cong Z, Liu Z, Qin Z, Zhang X, Zhang H, Li J, Yu H and Wang W 2015 *Opt. Laser Technol.* **73** 50

[32] Kaminskii A A, Pavlyuk A A, Kurbanov K, Ivannikova N V and Polyakova L A 1988 *Inorg. Mater.* **24** 1144

[33] Kaminskii A A, Kholov A, Klevtsov P V and Khafzov S K 1989 *Inorg. Mater.* **25** 890

[34] Kaminskii A A, Bagaev S N, Ueda K, Nishioka H, Kubota Y, Chen X and Kholov A 1995 *Japan. J. Appl. Phys.* **34** L1461

[35] Gi X, Lo Z, Huang Q, Liang J, Chen J, Huang Y, Qiu M and Zhang H 1989 *Phys. Status Solidi* a **114** K127

[36] Urata Y, Wada S, Tashiro H and Fukuda T 1999 *Appl. Phys. Lett.* **75** 636

[37] Kaminskii A A, Klassen N V, Red'kin B S, Eichler H and Findeisen J 1998 *Dokl.-Phys.* **43** 659

[38] Kaminskii A A *et al* 2000 *Opt. Commun.* **183** 277

[39] Chen W, Inagawa Y, Omatsu T, Tateda M, Takeuchi N and Usuki Y 2001 *Opt. Commun.* **194** 401

[40] Basiev T T, Karasik A Y, Sobol A A, Chunaev D S and Shukshin V E 2011 *Quantum. Electron.* **41** 370

[41] Zhang J-C, Yan L-Y, Xiao L, Zhang D-X and Feng B-H 2007 *Acta Phys. Sin.* **56** 2689

[42] Wang X, Fan Z, Yu H, Zhang H and Wang J 2017 *Opt. Mater. Express* **7** 1732

[43] Cerny P, Zverev P, Jelínkova H and Basiev T T 2000 *Opt. Commun.* **177** 397

[44] Sulc J, Jelínkova H, Basiev T T, Doroshenko M E, Ivleva L I, Osiko V V and Zverev P G 2007 *Opt. Mater.* **30** 195

[45] Pujol P C *et al* 2002 *Phys. Rev.* B **65** 165121

[46] Kloop P *et al* 2002 *Appl. Phys.* B **74** 185

[47] Rybakov V K, Trunov V K and Spitsin V I 1970 *Dokl.-Phys.* **192** 369

[48] Zhao W, Zhou W, Song M, Wang G, Du J, Yu H, Chen Y and Chen J 2011 *J. Cryst. Growth* **332** 87

[49] Kaminskii A A 1981/1990 *Laser Crystals, Their Physics and Properties* (Berlin: Springer)

[50] Kaminskii A A, Lux O, Rhee H, Eichler H J, Yoneda H, Shirakawa A, Bohatý L and Becker P 2014 *Laser Photonics. Rev.* **8** 324

[51] Damen T C, Porto S P S and Tell B 1966 *Phys. Rev.* **142** 570

[52] Rybakov V K and Trunov V K 1970 *Dokl. Chem.* **192** 2

[53] Trunov V K and Rybakov V K 1970 *Russ. J. Inorg. Chem.* **15** 546

[54] Rybakov V K and Trunov V K 1971 *Russ. J. Inorg. Chem.* **16** 1320

[55] Evdokimov A A and Trunov V K 1974 *Russ. J. Inorg. Chem.* **19** 232

[56] Borodko Y G, Shilova A K and Shilov A E 1970 *Russ. J. Inorg. Chem.* **44** 627

[57] Sarang S, Williams R J, Lux O, Kitzler O, McKay A, Jasbeer H and Mildren R P 2016 *Opt. Express* **24** 21463

[58] Liu J, Griebner U, Petrov V, Zhang H, Zhang J and Wang J 2005 *Opt. Lett.* **30** 2427

[59] Kaminskii A A, Dong J, Ueda K, Bettineli M, Grinberg M and Jaque D 2009 *Laser Phys. Lett.* **6** 782

[60] Li R, Bauer R and Lubeigt W 2013 *Opt. Express* **21** 17745

[61] Tang C Y, Zhuang W Z, Su K-W and Chen Y-F 2015 *IEEE J. Select. Top. Quantum Electron.* **21** 1400206

[62] Kaminskii A A 2017 *Dokl.-Phys.* **62** 450